

Phase sensitivity for an SU(1,1) interferometer via multiphoton subtraction at the output port

Tao Jiang¹, Zekun Zhao¹, Qingqian Kang^{1,2}, Teng Zhao¹, Nanrun Zhou³, Cunjin Liu^{1,*}, and Liyun Hu^{1,*}

¹Center for Quantum Science and Technology, Jiangxi Normal University, Nanchang 330022, China

²Department of Physics, College of Science and Technology,
Jiangxi Normal University, Nanchang 330022, China

³School of Electronic and Electrical Engineering, Shanghai University of Engineering Science, Shanghai 201620, China

In the field of quantum precision measurement, enhancing phase sensitivity is crucial for various applications, including quantum metrology and quantum sensing technologies. We theoretically investigate the improvement in phase sensitivity and quantum Fisher information achieved through multiphoton subtraction operations at the output port of an SU(1,1) interferometer under conditions of photon loss. We use vacuum and coherent states as the inputs and detect the outputs by intensity detection. The results indicate that internal photon losses within the SU(1,1) interferometer have a more significant impact on the phase sensitivity compared to external photon losses. Moreover, increasing the number of photon subtractions m effectively enhances both the phase sensitivity and the quantum Fisher information. Notably, even under conditions of severe photon loss, the multiphoton subtraction operations can enable the phase sensitivity to surpass the standard quantum limit, approaching both the Heisenberg limit and the quantum Cramér-Rao bound. This study provides a new theoretical basis for enhancing the phase sensitivity in the SU(1,1) interferometer.

PACS: 03.67.-a, 05.30.-d, 42.50.Dv, 03.65.Wj

I. INTRODUCTION

Quantum precision measurement is a significant branch of quantum metrology that utilizes quantum properties, such as quantum entanglement to achieve measurement accuracy that surpasses classical limits [1–8]. It provides unprecedented accuracy in estimating unknown physical parameters, which reveals widespread applications and rapid advancements in gravitational wave detection [9–11], optical imaging [12–14], biological measurements [15, 16], and fundamental physical experiments. However, a primary challenge is to attain an accuracy exceeding the standard quantum limit (SQL) [17, 18]. To address this challenge, researchers have been developing innovative techniques and schemes to further enhance the measurement accuracy and sensitivity [19–22].

Generally, the process of quantum precision measurement can be divided into three stages: the preparation of quantum states, the interaction between the interferometers and the input states, and finally, the measurement stage [23]. Researchers have been focusing on optimizing these stages to achieve higher measurement accuracy. In classical theory, the measurement limit is known as the SQL, which is defined by $1/\sqrt{N}$, where N represents the average number of photons contributing to the measurement [7, 24, 25]. To achieve the phase sensitivity that surpasses the SQL, various non-classical states such as entangled states [26], NOON states [27], and twin Fock states, have been proposed as the light sources in the measurement [28]. Numerous studies have examined the use of non-classical states to enhance the

phase sensitivity of interferometers. For instance, Caves proposed that introducing a squeezed vacuum state as the input for the Mach-Zehnder interferometer (MZI) can enhance phase sensitivity, allowing measurement accuracy to exceed the SQL [7]. However, high-quality non-classical states are not only difficult to generate but also highly susceptible to environmental noise. Consequently, utilizing the quantum properties of non-classical states to improve measurement accuracy in noisy environments has become a significant focus of research [29–31]. For example, Xu *et al.* proposed utilizing photon-added squeezed vacuum state and coherent state as inputs for the SU(1,1) interferometer. Their research indicated that this approach can surpass the SQL for phase sensitivity even in the presence of photon losses [32]. Similarly, Gong *et al.* proposed a scheme that employs photon-subtracted squeezed vacuum state and coherent state as inputs for the SU(1,1) interferometer, revealing significantly improved phase sensitivity due to enhanced internal correlations within the interferometer [33]. Thus, the choice of input states plays a crucial role in influencing measurement accuracy.

On the other hand, in the interaction process between quantum states and interferometers, common MZI and SU(1,1) interferometer are employed. A typical MZI consists of two 50:50 beam splitters (BSs) [30, 34, 35], while a standard SU(1,1) interferometer is composed of two optical parametric amplifiers (OPAs) [20–22, 35]. As nonlinear optical devices, OPAs are capable of generating quantum entanglement, which significantly enhances both the signal-to-noise ratio and the phase sensitivity, thereby making them highly effective in precision measurement applications [5, 20, 21]. Notably, several studies have demonstrated that combining an MZI with an SU(1,1) interferometer can yield excellent results in terms of phase sensitivity [36–38]. Furthermore,

* Corresponding authors: lcjwelldone@126.com, hlyun@jxnu.edu.cn

extensive investigations have been conducted on the use of various configurations and different types of phase shifters to enhance the phase sensitivity of interferometers [39–43]. Given the advantages of the SU(1,1) interferometer, it has garnered considerable attention in both theoretical and experimental research [44–47].

Although the SU(1,1) interferometer has demonstrated significant advantages in phase estimation, studies by Stuart S. Szigeti *et al.* indicate that only particles coupled through pumping contribute to the phase sensitivity in the SU(1,1) interferometer, and the number of particles involved is relatively small [47]. To address this issue, researchers have increasingly focused on performing non-Gaussian operations at the output port of SU(1,1) interferometers to optimize phase encoding processes. Notably, Zhang *et al.* investigated the enhancement of phase sensitivity through single-photon subtraction at the output port of the SU(1,1) interferometer under ideal conditions [37]. To examine the impact of the single-photon subtraction at the output on quantum Fisher information (QFI), they proposed a non-Gaussian equivalent probe state that incorporates the effects of the photon subtraction into the input state. In their approach, the equivalent probe state relies on the unknown phase ϕ to be measured. However, preparing such an input state using prior photon subtraction or addition schemes is not feasible, especially for an unknown phase-related case. To resolve this issue, we propose an equivalent model in which the effects of the photon subtraction do not need to be incorporated into the input state, allowing it to remain independent of the unknown phase ϕ , resulting in more reliable measurements. Our approach differs from that of Zhang *et al.* in several key aspects. First, our proposed equivalent model does not necessitate modifications to the input states and is entirely based on the standard SU(1,1) interferometer, making it more comprehensible and practical. Furthermore, while Zhang *et al.* focused on the single-photon subtraction under ideal conditions, we emphasize the crucial role of the multi-photon subtraction in the presence of photon losses.

Our paper is organized as follows: In Sec. II, we introduce our model. In Sec. III, we explore the enhancement of phase sensitivity in the SU(1,1) interferometer through the multiphoton subtraction operations, considering both ideal conditions and photon loss scenarios. In Sec. IV, we calculate the QFI in the presence of photon losses and compare the phase sensitivity with theoretical limits. Finally, in Sec. V, we present our conclusions.

II. MODEL

Our model is based on the standard SU(1,1) interferometer which consists of two OPAs and a linear phase shifter, as illustrated in Fig. 1. In this model, the input states comprise a vacuum state $|0\rangle_a$ and a coherent state $|\beta\rangle_b$ (where $\beta = |\beta|e^{i\theta_\beta}$, with θ_β representing the phase).

The input state can be expressed as $|\psi\rangle_{in} = |0\rangle_a \otimes |\beta\rangle_b$. Mode a propagates through the two OPAs and the linear phase shifter. The multiphoton subtraction operations are implemented at the output port, and the phase sensitivity is measured using intensity detection. Mode b neither undergoes the phase shifter nor the multiphoton subtraction operations. We illustrate the operational process of the interferometer using mode a as an example. The OPA process can be represented by the two-mode squeezing operator $S_k^\dagger(\xi_k) = \exp(\xi_k ab - \xi_k a^\dagger b^\dagger)$, where $\xi_k = g_k e^{i\theta_k}$ denotes the squeezing parameter, with g_k and θ_k representing the gain factor and phase of the OPA, respectively, with $k = 1, 2$. The operators a (a^\dagger) and b (b^\dagger) correspond to the annihilation (creation) operators for the two modes. The phase shifter is described by the unitary operator $U_\phi = e^{i\phi a^\dagger a}$, where ϕ denotes the phase shift. Finally, we perform intensity detection at the output port of mode a .

For simplicity, we consider the parameters under the balance condition. For the two OPAs, the balance condition is defined as $\theta_1 = 0$, $\theta_2 = \pi$, and $g_1 = g_2 = g$ [48]. For the input coherent state of mode b ($|\beta\rangle_b$), the phase shift balance condition is $\theta_\beta = 0$.



FIG. 1. Schematic diagram of our model based on SU(1,1) interferometer. The two input ports of this interferometer are a vacuum state $|0\rangle_a$ and a coherent state $|\beta\rangle_b$. OPA stands for optical parametric amplifier, ϕ is the phase shift, and D_a is the intensity detector. The operator a^m represents the subtraction of m photons.

After undergoing a series of operations, the output state of mode a before detection can be expressed as

$$|\psi\rangle_{out} = N_1 a^m S_2 U_\phi S_1 |\psi\rangle_{in}, \quad (1)$$

where N_1 is the normalization coefficient, which can be calculated as [32]

$$N_1 = (G_m e^{A_1})^{-\frac{1}{2}}, \quad (2)$$

and

$$G_m e^{(\cdot)} = \frac{\partial^{2m}}{\partial t^m \partial s^m} e^{(\cdot)} \Big|_{t=s=0}, \quad (3)$$

$$A_1 = st |w_1|^2 + (tw_1 + sw_1^*) \beta, \quad (4)$$

as well as

$$w_1 = \frac{1}{2} \sinh 2g (1 - e^{-i\phi}). \quad (5)$$

Here, m represents the number of the photon subtraction operations, while s and t are differential variables. After differentiation, these variables become 0.

At the end of this section, we briefly discuss the feasibility of our approach. In recent years, extensive research has focused on employing non-Gaussian operations to enhance the phase sensitivity [49–54]. Dakna *et al.* proposed that photon-added states, such as photon-added thermal states, squeezed states, coherent states, and displaced photon-number states, could be realized through conditional output measurements at a BS [55]. Furthermore, Namekata *et al.* have experimentally demonstrated the photon subtraction operations using pulsed squeezing at telecommunications wavelengths [49]. Therefore, our proposed schemes are feasible for implementing the photon subtraction operations.

III. PHASE SENSITIVITY BASED ON INTENSITY DETECTION

A. Phase sensitivity in ideal case

To discuss the phase sensitivity, three common detection methods are used, i.e., intensity detection [32, 34, 56], homodyne detection [57], and parity detection [22, 28, 30]. Notably, intensity detection is both experimentally feasible and straightforward for theoretical calculations. Consequently, in this section, we employ intensity detection at the output port of mode a to estimate the phase sensitivity, which can be determined using the error propagation formula [35]

$$\Delta^2\phi = \frac{\langle N^2 \rangle - \langle N \rangle^2}{|\partial_\phi \langle N \rangle|^2}. \quad (6)$$

In this equation, $\langle N \rangle = {}_{out} \langle \psi | a^\dagger a | \psi \rangle_{out}$, where N represents the number operator. According to Eq. (6), we can obtain the phase sensitivity as follows (for detailed computation process, see Appendix A) [32]

$$\Delta^2\phi = \frac{N_1^2}{|\partial_\phi (N_1^2 G_{m+1} e^{A_1})|^2} \times [G_{m+1} e^{A_1} + G_{m+2} e^{A_1} - N_1^2 (G_{m+1} e^{A_1})^2]. \quad (7)$$

To investigate the influence of the multiphoton subtraction operations on the phase sensitivity, we plot the phase sensitivity $\Delta\phi$ as a function of ϕ as shown in Fig. 2. Here, the variable m denotes the number of the photon

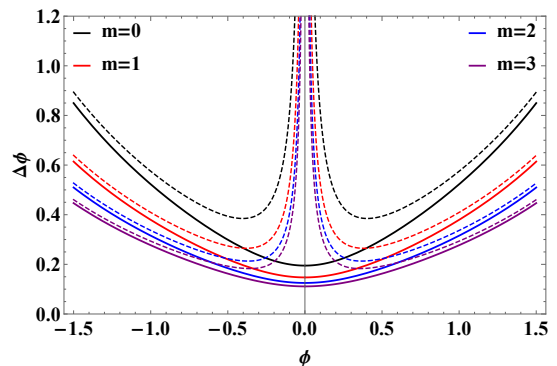


FIG. 2. The phase sensitivity based on intensity detection as a function of ϕ with $\beta = 1$, $g = 1$. The solid line and the dashed line represent the detection of mode a and mode b , respectively. m is the number of the photon subtraction operations.

subtraction operations, with solid and dashed lines representing detections at ports a and b , respectively. From Fig. 2, we can get the following conclusions: (i) when the parameters are chosen identically, the detection results at port a outperform those at port b ; (ii) at the same phase point, the phase sensitivity improves as m increases; (iii) the intensity detection results for mode a indicate that the optimal phase sensitivity occurs near the phase point $\phi = 0$, whereas this is not the case for mode b ; (iv) when the phase shift is large, the phase sensitivity detected at both ports is similar, but the advantage is still kept by mode a .

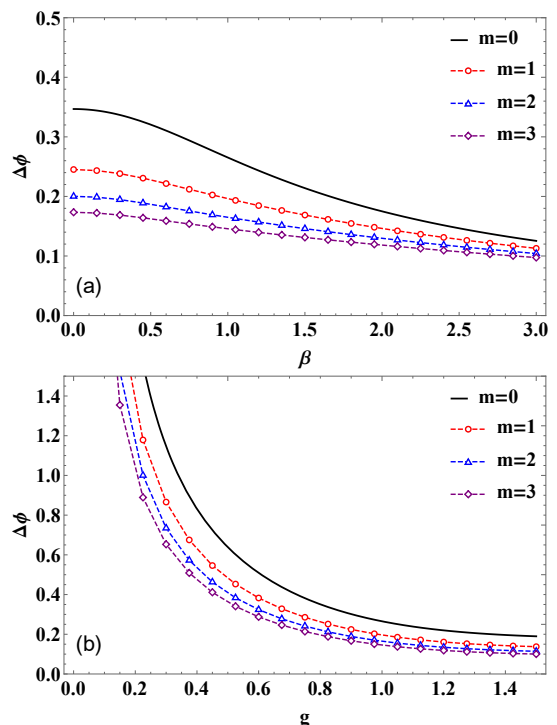


FIG. 3. The phase sensitivity based on intensity detection as a function of (a) β , $g = 1$, $\phi = 0.4$; and (b) g , $\beta = 1$, $\phi = 0.4$.

Next, we explore the influence of other parameters on the phase sensitivity of the interferometer. Given that the optimal phase point under conditions of photon loss is not near $\phi = 0$, we will uniformly select $\phi = 0.4$ for the purposes of comparison in the following discussion. Fig. 3 illustrates the variations in the phase sensitivity $\Delta\phi$ with respect to the coherent state amplitude β of mode b and the amplification coefficient g of the OPA. From Fig. 3, it is evident that: (i) the phase sensitivity improves with β , attributing to the increase in the number of photons entering the interferometer, which enhances the energy of the light field, thereby enhancing the phase sensitivity. Notably, this enhancement is more pronounced at lower values of β , indicating that a relatively low energy input is sufficient to achieve a high level of the phase sensitivity; (ii) at a constant β , the phase sensitivity improves with m . Similar results can be obtained for the case of gain factor g , see Fig. 3(b). This improvement can be attributed to the OPA amplifying the signal power of the input light. As g increases, the OPA enhances the amplification effect on the input signal, resulting in a more robust output signal from the interferometer and thereby enhancing the phase sensitivity.

As illustrated in Figs. 2 and 3, it is evident that the multiphoton subtraction operations significantly enhance the phase sensitivity of the SU(1,1) interferometer under ideal conditions. This improvement primarily arises from the multiphoton subtraction operations, which result in an increased photon count detected at the output port. Consequently, this enhancement significantly improves both the signal strength and the signal-to-noise ratio, thereby facilitating more accurate measurements of phase changes.

B. Phase sensitivity in the presence of photon losses

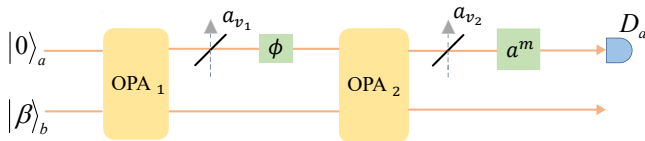


FIG. 4. Schematic diagram of the photon losses; adding fictitious BSs to simulate photon losses inside and outside the SU(1,1) interferometer.

The preceding discussion is based on ideal conditions; however, in practical applications, losses cannot be overlooked. Thus, we will analyze the effects of both internal and external photon losses on the phase sensitivity separately. We assume that photon losses occur between the first OPA and the phase shifter, which we regard as internal losses. Conversely, photon losses that occur between the second OPA and the multiphoton subtraction operations are considered external losses, as shown in Fig. 4.

To simulate these loss processes, we introduce fictitious BSs, and their transformation relations are expressed as

$$B_k^\dagger a_k B_k = \sqrt{T_k} a_k + \sqrt{1 - T_k} a_{v_k}, \quad (8)$$

where B_k is the BS operator, a_{v_k} is the vacuum noise operator corresponding to mode a , and T_k denotes the transmittance of the BSs. When $T_k = 1$, it indicates no loss; when $T_k = 0$, it indicates a hundred percent loss, with $k = 1, 2$.

In the model that accounts for photon losses, the relationship between the output state and the input state is given by

$$|\psi\rangle_{out} = N_2 a^m B_2 S_2 U_\phi B_1 S_1 |\psi\rangle_{in} |0\rangle_{a_{v_1}} |0\rangle_{a_{v_2}}, \quad (9)$$

where N_2 is the normalization coefficient, and it can be expressed as

$$N_2 = (G_m e^{A_2})^{-\frac{1}{2}}. \quad (10)$$

Based on Eqs. (6), (8) and (9), we can obtain the phase sensitivity $\Delta^2\phi_L$ under photon losses, i.e.,

$$\Delta^2\phi_L = \frac{N_2^2}{|\partial_\phi (N_2^2 G_{m+1} e^{A_2})|^2} \times [G_{m+1} e^{A_2} + G_{m+2} e^{A_2} - N_2^2 (G_{m+1} e^{A_2})^2], \quad (11)$$

where

$$A_2 = st |w_3|^2 + (tw_3 + sw_3^*) \beta, \quad (12)$$

and

$$w_3 = \frac{1}{2} \sinh 2g \sqrt{T_2} (1 - \sqrt{T_1} e^{-i\phi}). \quad (13)$$

From Eqs. (11)-(13), it is evident that when $T_1 = T_2 = 1$, the phase sensitivity with photon losses returns to that of the ideal case. Next, we will explore the effects of internal ($T_2 = 1, T_1 = T$) and external ($T_1 = 1, T_2 = T$) photon losses on the phase sensitivity separately. Fig. 5 illustrates the variation of the phase sensitivity $\Delta\phi_L$ as a function of T in the presence of photon losses. From Fig. 5, we can draw the following conclusions: (i) both internal and external photon losses adversely affect the phase sensitivity; however, internal photon losses have a more significant impact, particularly at lower T . This can be attributed to the model, as photon losses inside the interferometer are amplified by the second OPA, whereas external losses are not, resulting in a more pronounced effect of internal losses on the phase sensitivity; (ii) the photon subtraction operations can enhance the phase

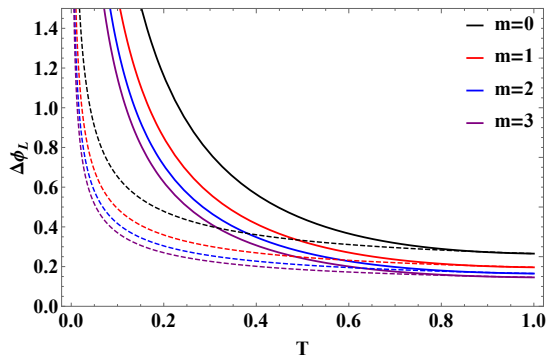


FIG. 5. The phase sensitivity based on intensity detection as a function of T with $\beta = 1$, $\phi = 0.4$, and $g = 1$. The solid and the dashed lines represent the conditions with internal and external photon losses, respectively.

sensitivity of the SU(1,1) interferometer in a noisy environment, with the degree of improvement increasing with the number of photons subtracted.

From the above discussion, it is clear that internal photon losses within the interferometer significantly affect the phase sensitivity in our model. Consequently, we will focus on the case of internal photon losses in the subsequent analysis.

IV. QFI AND THEORETICAL LIMITS

A. QFI in ideal case

The QFI is a crucial metric for assessing the maximum information contained in an unknown phase shift ϕ , within the realm of quantum precision measurement. The quantum Cramér-Rao bound (QCRB) associated with the QFI represents the ultimate theoretical limit for phase measurement. This bound is independent of the detection method employed, and for fixed input resources, the QFI remains constant. In the ideal case, for a pure state as the input, the QFI is given by

$$F = 4 \left[\langle \psi'_\phi | \psi'_\phi \rangle - \left| \langle \psi'_\phi | \psi_\phi \rangle \right|^2 \right], \quad (14)$$

and the QCRB is given by

$$\Delta\phi_{QCRB} = \frac{1}{\sqrt{\nu F}}, \quad (15)$$

where ν represents the number of repeated experiments. For simplicity, we set $\nu = 1$.

Here, $|\psi_\phi\rangle$ represents the state after undergoing a phase shift. In our model, to account for the influence of the multiphoton subtraction operations on the ideal QFI, we construct an equivalent model (see Fig. 6). In this model, we introduce a non-local operation

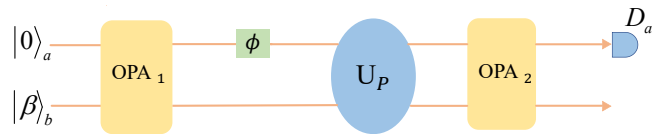


FIG. 6. Schematic diagram of the equivalent model of the SU(1,1) interferometer, where U_P represents a non-local operation, and $U_P = S_2^\dagger a^m S_2$.

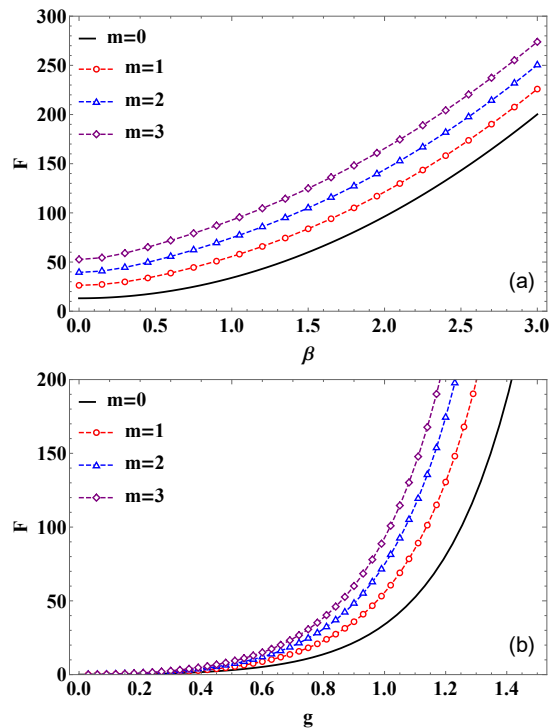


FIG. 7. The quantum Fisher information F as a function of (a) β with $g = 1$, and $\phi = 0.4$, and (b) g with $\beta = 1$, and $\phi = 0.4$.

(U_P), where $U_P = S_2^\dagger a^m S_2$. The multiphoton subtraction operations are incorporated as part of the non-local operation, and we have $|\psi_\phi\rangle = N_1 U_P U_\phi S_1 |\psi\rangle_{in}$, with $|\psi'_\phi\rangle = \partial |\psi_\phi\rangle / \partial \phi$. For simplicity, we provide the calculated result of the QFI under ideal conditions in Appendix B.

In Fig. 7, we illustrate the variation of the QFI with respect to β and g under ideal conditions. It is evident that the QFI increases with both β and g . This increase can be attributed to the fact that as β and g increase, the number of photons within the interferometer also rises, thereby enhancing the interference effects. The reduction in system uncertainty facilitates stronger interference effects, enabling the interferometer to extract more information, which in turn enhances the QFI. Furthermore, when other parameters are the same, the QFI increases with the number of the photon subtractions. The magnitude of the QFI is closely related to the non-classicality of the quantum states. Non-Gaussian

operations such as photon subtraction can enhance the non-classical properties of the quantum states, including quantum statistics, quantum entanglement, and quantum coherence, ultimately leading to an increase in the QFI.

Fig. 8 illustrates the variation of the phase sensitivity $\Delta\phi$ and $\Delta\phi_{QCRB}$ under ideal conditions as the parameters β and g increase. It is evident that the phase sensitivity $\Delta\phi$ improves as β and g increase, with $\Delta\phi_{QCRB}$ following a similar trend. The enhancement is more pronounced at lower values of these parameters. Furthermore, the multiphoton subtraction operations significantly enhance both the phase sensitivity $\Delta\phi$ and $\Delta\phi_{QCRB}$. However, since the QCRB represents the theoretical limit of the parameter estimation accuracy, when m is fixed, the dashed lines of the same color are consistently below the corresponding solid lines. This observation indicates that while our method can bring the phase sensitivity $\Delta\phi$ close to $\Delta\phi_{QCRB}$ under ideal conditions, it cannot fully achieve this limit, which is consistent with the principles of quantum limit theory.

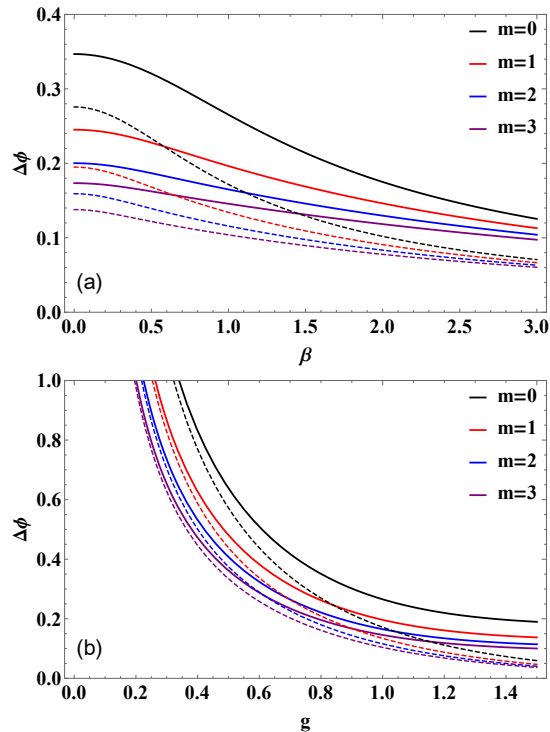


FIG. 8. The phase sensitivity and QCRB as a function of (a) β with $g = 1$, and $\phi = 0.4$, and (b) g with $\beta = 1$, and $\phi = 0.4$. The solid line and dashed line represent the phase sensitivity $\Delta\phi$ and $\Delta\phi_{QCRB}$, respectively.

B. QFI in the presence of photon losses

Next, we further explore the influence of photon losses on the QFI. In our model, the phase shifter induces a mi-

nor phase shift within mode a . For simplicity, we concentrate solely on photon losses occurring within mode a inside the interferometer, as shown in Fig. 9. Furthermore, we will compute the QFI in the presence of photon losses utilizing the method proposed by Escher *et al.* [3]. For additional details regarding the calculation, please refer to Appendix C.

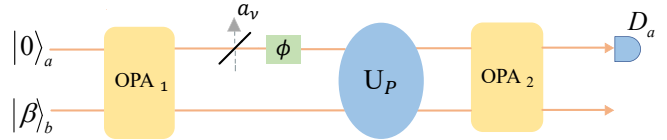


FIG. 9. Schematic diagram of the photon losses on mode a , where U_P represents a non-local operation, and $U_P = S_2^\dagger a^m S_2$.

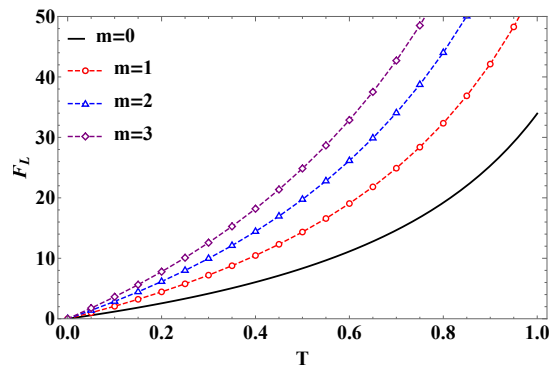


FIG. 10. The quantum Fisher information F as a function of T with $\beta = 1$, $g = 1$, and $\phi = 0.4$.

Fig. 10 illustrates the variation of the QFI with the transmissivity T of the BS that simulates photon losses. It is evident that: (i) photon losses significantly impact the QFI; as photon losses increase, the QFI correspondingly decreases. This reduction can be attributed to the diminished number of photons participating in the interference within the SU(1,1) interferometer due to these losses, thereby reducing the amount of information obtainable within the interferometer and ultimately leading to a decrease in the QFI; (ii) when photon losses remain constant, the QFI increases with m . This indicates that the multiphoton subtraction operations enhance the non-classicality of the quantum state, improving the phase sensitivity of the light field and rendering the quantum state more sensitive to the phase changes. Based on Eq. (14), the QFI quantitatively describes the sensitivity of a quantum state to phase changes; thus, the increase in phase sensitivity directly results in a higher QFI. Therefore, this demonstrates that the multiphoton subtraction operations can effectively mitigate the impact of internal photon losses in the interferometer on the QFI.

Meanwhile, Fig. 11 illustrates the variation of the QFI with respect to the parameters β and g under conditions of photon loss. It is evident that when β and g are within

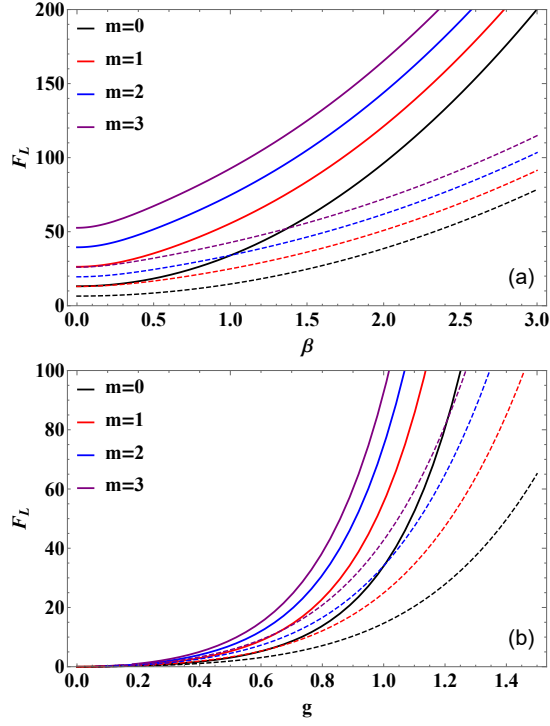


FIG. 11. The quantum Fisher information F as a function of (a) β with $g = 1$, and $\phi = 0.4$, and (b) g with $\beta = 1$, and $\phi = 0.4$. The solid line and dashed line correspond to the ideal case ($T = 1$) and the photon losses case ($T = 0.7$), respectively.

a specific range, a 30% photon losses ($T = 0.7$) result in a reduction of over 50% in the QFI, demonstrating the significant impact of photon losses on the QFI. Furthermore, in Figs. 11(a) and 11(b), intersections can be observed between the black solid line and the three dashed lines in red, blue, and purple. This indicates that the effects of photon losses on the QFI can be mitigated through the implementation of the multiphoton subtraction operations.

C. Phase sensitivity compared with theoretical limits

In this subsection, we further illustrate the advantages of our approach by comparing the phase sensitivity of the interferometer with several theoretical limits, specifically in the presence of internal photon losses. These limits include the SQL, the Heisenberg limit (HL), and the QCRB.

SQL and HL are associated with the internal mean photon number of the interferometer (N_T), which can be expressed as

$$\Delta\phi_{SQL} = \frac{1}{\sqrt{N_T}}, \quad (16)$$

$$\Delta\phi_{HL} = \frac{1}{N_T}. \quad (17)$$

In our model, to account for the effects of the multi-

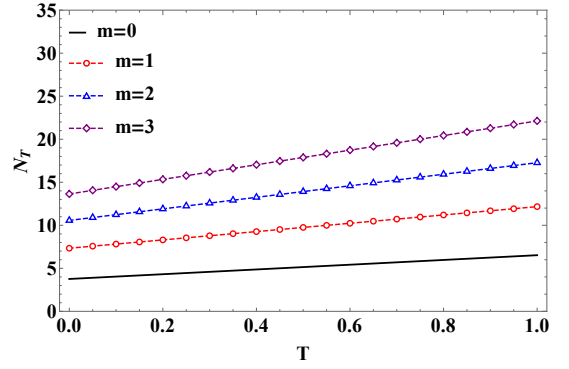


FIG. 12. The average photon number N as a function of T , with $\beta = 1$, $g = 1$, and $\phi = 0.4$.

photon subtraction operations at the output port of the interferometer on the SQL and the HL, we use the photon count prior to the final OPA in the model shown in Fig. 9 to calculate the average photon number within the interferometer. The expression for N_T is given by

$$N_T = {}_{int} \langle \psi | (a^\dagger a + b^\dagger b) | \psi \rangle_{int}, \quad (18)$$

where $|\psi\rangle_{int} = N_4 U_P U_\phi B_1 S_1 |0\rangle_a |\beta\rangle_b$, and N_4 is the normalization coefficient. Further computational details can be found in Appendix D.

Next, we further examine the impact of the multiphoton subtraction operations on the average photon number within the interferometer. As shown in Fig. 12, these operations significantly increase the average photon number, thereby enhancing the quantity of photons that carry phase information. This finding contrasts with the conventional understanding that photon subtraction typically reduces the number of photons. We interpret photon subtraction as a probabilistic non-Gaussian operation. When the photon number distribution of the input state is super-Poissonian, performing photon subtraction leads to an output state characterized by an increased average photon number. Moreover, in scenarios where photon losses are relatively low, the multiphoton subtraction operations demonstrate a more pronounced increase in photon number, suggesting that our approach is particularly effective under low-loss conditions. Additionally, the SQL and the HL are correlated with the average number of photons present within the interferometer. Consequently, the multiphoton subtraction operations enhance the quantum theoretical limits.

In Fig. 13, we present curves that illustrate the phase sensitivity and the corresponding theoretical limits for $m = 0, 1, 2$, and 3 as functions of the transmittance T . It is evident from Fig. 13 that: (i) the multiphoton subtraction operations enhance the phase sensitivity while simultaneously improving the theoretical precision limit. Our scheme demonstrates that the phase sensitivity can surpass the SQL even when photon losses reach 40%, highlighting the robustness of the approach; (ii) photon

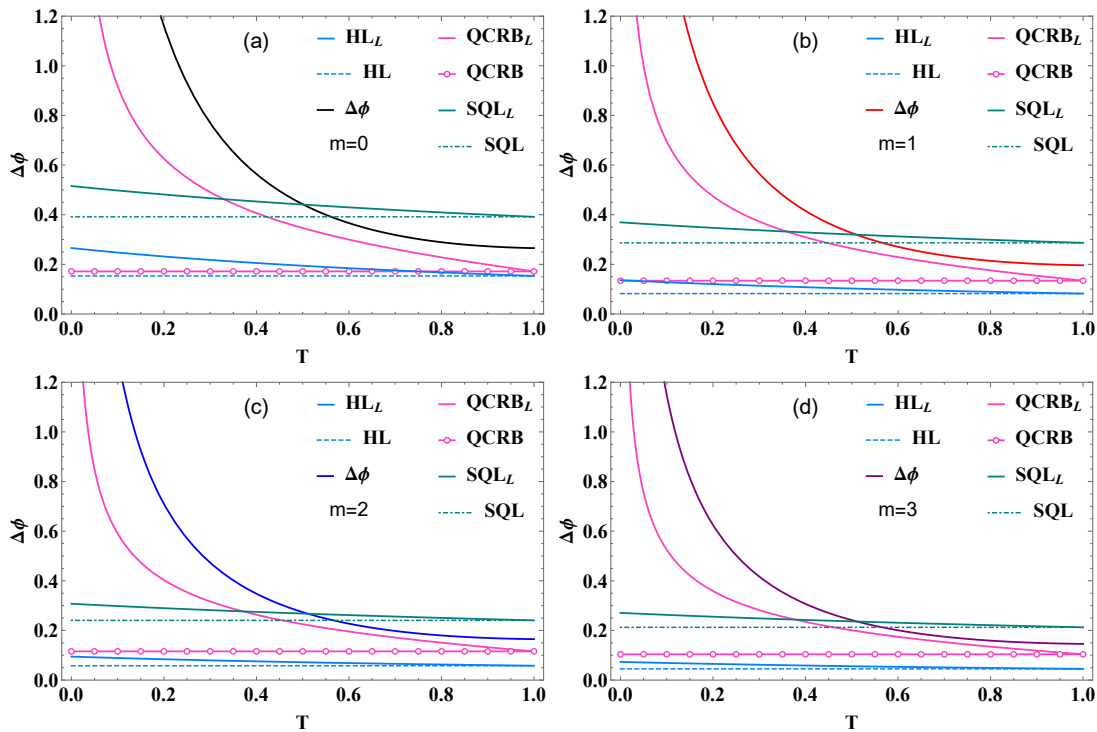


FIG. 13. The phase sensitivity and theoretical limits as a function of T with $\beta = 1$, $g = 1$, and $\phi = 0.4$. The subtracting of 0, 1, 2, and 3 photons corresponds to (a), (b), (c), and (d), respectively.

losses in mode a within the interferometer significantly impact the QCRB but have a lesser effect on the SQL and the HL; (iii) in our scheme, the HL precision exceeds the QCRB precision under ideal conditions. Furthermore, as m increases, the phase sensitivity approaches the QCRB more closely in the presence of photon losses.

V. CONCLUSION

In this paper, we investigate the effects of the multiphoton subtraction operations at the output port of the SU(1,1) interferometer on the phase sensitivity. Our study utilizes vacuum and coherent states as the inputs, employing intensity detection as the measurement method. We first explore the impact of various orders of the photon subtraction operations on the phase sensitivity under ideal conditions, revealing that an increase in the number of photon subtractions gradually enhances the phase sensitivity. Additionally, we compare the phase sensitivity obtained from detections at the a and b ports of the interferometer, finding that detection at the a port is more effective.

We also examine the effects of photon losses on the phase sensitivity and the QFI. Our analysis reveals that internal photon losses in the SU(1,1) interferometer have a more pronounced impact on the phase sensitivity compared to external losses. Furthermore, to assess the impact of the photon subtraction operations at the output

port on the QFI, we propose an equivalent model that treats the multiphoton subtraction operations as part of a non-local operation. The results indicate that even under relatively severe photon losses, our method significantly improves both the phase sensitivity and the QFI. Finally, we compare the phase sensitivity with the theoretical limits under conditions of photon loss, demonstrating that our approach enables the phase sensitivity to surpass the SQL while also approaching the HL and the QCRB even with 40% photon losses. Overall, our research provides theoretical support for the advancement of quantum information science.

ACKNOWLEDGMENTS

This work is supported by the National Natural Science Foundation of China (Grants No. 11964013 and No. 12104195) and the Jiangxi Provincial Natural Science Foundation (Grants No. 20242BAB26009 and 20232BAB211033), Jiangxi Provincial Key Laboratory of Advanced Electronic Materials and Devices (Grant No. 2024SSY03011), as well as Jiangxi Civil-Military Integration Research Institute (Grant No. 2024JXRH0Y07).

APPENDIX A : PHASE SENSITIVITY IN IDEAL CASE

In this Appendix, we provide the formula for the phase sensitivity under ideal conditions. By following a series

of operations, the output state can be expressed as follows

$$|\psi\rangle_{out} = N_1 a^m S_2 U_\phi S_1 |\psi\rangle_{in}. \quad (\text{A1})$$

Before deriving the phase sensitivity, we first introduce a formula, i.e.,

$$\begin{aligned} & S_1^\dagger U_\phi^\dagger S_2^\dagger a^{\dagger m} a^m S_2 U_\phi S_1 \\ &= \frac{\partial^{2m}}{\partial t^m \partial s^m} [S_1^\dagger U_\phi^\dagger S_2^\dagger \exp(ta^\dagger) \\ &\times \exp(sa) S_2 U_\phi S_1] |_{t=s=0} \\ &= \frac{\partial^{2m}}{\partial t^m \partial s^m} [\exp(tw_2 a^\dagger) \exp(tw_1 b) \\ &\times \exp(sw_2^* a) \exp(sw_1^* b^\dagger)] |_{t=s=0}, \end{aligned} \quad (\text{A2})$$

where we have set

$$w_1 = \frac{1}{2} \sinh 2g (1 - e^{-i\phi}), \quad (\text{A3})$$

$$w_2 = \cosh^2 g e^{-i\phi} - \sinh^2 g, \quad (\text{A4})$$

According to the normalization condition, we have

$$\begin{aligned} & \text{out} \langle \psi | \psi \rangle_{out} \\ &= N_1^2 \text{in} \langle \psi | S_1^\dagger U_\phi^\dagger S_2^\dagger a^{\dagger m} a^m S_2 U_\phi S_1 |\psi\rangle_{in} \\ &= N_1^2 \frac{\partial^{2m}}{\partial t^m \partial s^m} \{ \exp[t(w_2 a^\dagger + w_1 b)] \\ &\times \exp[s(w_2^* a + w_1^* b^\dagger)] \} |_{t=s=0} \\ &= N_1^2 G_m e^{A_1} \\ &= 1, \end{aligned} \quad (\text{A5})$$

where

$$G_m e^{(\cdot)} = \frac{\partial^{2m}}{\partial t^m \partial s^m} e^{(\cdot)} |_{t=s=0}, \quad (\text{A6})$$

and

$$A_1 = st |w_1|^2 + (tw_1 + sw_1^*) \beta, \quad (\text{A7})$$

$$N_1 = (G_m e^{A_1})^{-\frac{1}{2}}. \quad (\text{A8})$$

Here, m is an integer representing the number of the photon subtractions, while s and t are differential variables. After differentiation, these variables all become 0.

Then, based on Eqs. (A1)-(A8), the phase sensitivity in the ideal case is given by

$$\Delta^2 \phi = \frac{\langle N^2 \rangle - \langle N \rangle^2}{|\partial_\phi \langle N \rangle|^2}, \quad (\text{A9})$$

where

$$\langle N \rangle =_{out} \langle \psi | a^\dagger a | \psi \rangle_{out} = N_1^2 G_{m+1} e^{A_1}, \quad (\text{A10})$$

and

$$\begin{aligned} \langle N^2 \rangle &=_{out} \langle \psi | (a^\dagger a)^2 | \psi \rangle_{out} \\ &= N_1^2 (G_{m+1} e^{A_1} + G_{m+2} e^{A_1}). \end{aligned} \quad (\text{A11})$$

APPENDIX B : QFI UNDER IDEAL CONDITION

To calculate the ideal QFI, we introduce an equivalent model shown in Fig. 6. According to Eq. (14), we have $|\psi_\phi\rangle = N_1 U_P U_\phi S_1 |0\rangle_a \otimes |\beta\rangle_b$, with $U_P = S_2^\dagger a^m S_2$, and derived $|\psi'_\phi\rangle = \frac{\partial |\psi_\phi\rangle}{\partial \phi}$. Then, the QFI in the ideal case is given by

$$F = 4 \left[\langle \psi'_\phi | \psi'_\phi \rangle - \left| \langle \psi'_\phi | \psi_\phi \rangle \right|^2 \right], \quad (\text{B1})$$

with

$$\begin{aligned} \langle \psi'_\phi | \psi'_\phi \rangle &= N_1^2 Y_m e^{F_1} + \left(\frac{\partial N_1}{\partial \phi} \right)^2 G_m e^{F_2} \\ &\quad + i N_1 \frac{\partial N_1}{\partial \phi} H_m e^{F_4} - i N_1 \frac{\partial N_1}{\partial \phi} H_m e^{F_3}, \end{aligned} \quad (\text{B2})$$

$$\langle \psi'_\phi | \psi_\phi \rangle = -i N_1^2 H_m e^{F_3} + \frac{\partial N_1}{\partial \phi} N_1 G_m e^{F_2}, \quad (\text{B3})$$

$$\langle \psi_\phi | \psi'_\phi \rangle = i N_1^2 H_m e^{F_4} + \frac{\partial N_1}{\partial \phi} N_1 G_m e^{F_2}, \quad (\text{B4})$$

where we have defined

$$H_m e^{(\cdot)} = \frac{\partial^{2m+2}}{\partial t^m \partial s^m \partial c \partial d} e^{(\cdot)} |_{t=s=c=d=0}, \quad (\text{B5})$$

$$Y_m e^{(\cdot)} = \frac{\partial^{2m+4}}{\partial t^m \partial s^m \partial c \partial d \partial p \partial h} e^{(\cdot)} |_{t=s=c=d=p=h=0}. \quad (\text{B6})$$

Here, m is an integer representing the number of the photon subtractions, while $s, t, c, d, p,$ and h are differential variables. After differentiation, these variables all become 0.

In addition, we have set

$$\begin{aligned} F_1 &= df_1^* (tf_3 + pf_1) + spf_1 f_3^* + ph |f_2|^2 \\ &\quad + tf_4 (sf_4^* + hf_2^*) + cf_2 (sf_4^* + hf_2^* + df_2^*) \\ &\quad + (sf_4^* + hf_2^* + df_2^* + cf_2 + tf_4 + pf_2) \beta, \end{aligned} \quad (\text{B7})$$

$$F_2 = st |f_4|^2 + (sf_4^* + tf_4) \beta, \quad (\text{B8})$$

$$\begin{aligned} F_3 &= tdf_1^* f_3 + cd |f_2|^2 + st |f_4|^2 + csf_2 f_4^* \\ &\quad + (df_2^* + sf_4^* + cf_2 + tf_4) \beta, \end{aligned} \quad (\text{B9})$$

$$\begin{aligned} F_4 &= csf_1 f_3^* + st |f_4|^2 + cd |f_2|^2 + tdf_2^* f_4 \\ &\quad + (sf_4^* + df_2^* + tf_4 + cf_2) \beta, \end{aligned} \quad (\text{B10})$$

with

$$\begin{aligned}
f_1 &= \cosh g e^{-i\phi}, \\
f_2 &= -\sinh g e^{-i\phi}, \\
f_3 &= \cosh^2 g e^{-i\phi} - \sinh^2 g, \\
f_4 &= \frac{1}{2} \sinh 2g (1 - e^{-i\phi}).
\end{aligned} \tag{B11}$$

APPENDIX C : QFI in the presence of photon losses

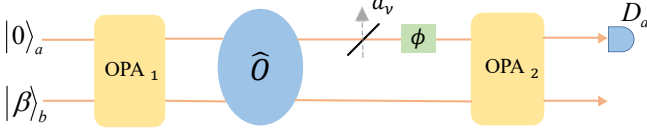


FIG. 14. Schematic diagram of the photon losses on mode a , where \hat{O} represents a non-local operation, and $\hat{O} = \frac{\partial^m}{\partial s^m} \exp [s (ae^{i\phi} \sqrt{\eta} \cosh g + b^\dagger \sinh g)] |_{s=0}$.

In this section, we further derive the QFI in the presence of photon losses within the system, as shown in Fig. 9. It is crucial to emphasize that for the $SU(1,1)$ interferometer, the QFI quantifies the amount of information acquired before the final OPA. Consequently, we focus on the quantum state before the second OPA. We denote the initial probe state of the $SU(1,1)$ interferometer system S as $|\psi\rangle_S = S_1 |0\rangle_a \otimes |\beta\rangle_b$. Due to photon losses in the system, the process of encoding the unknown phase into the probe state $|\psi\rangle_S$ is no longer a unitary evolution. Therefore, we transform the problem into parameter estimation under unitary evolution in an extended system $S + E$. In this extended system, the probe state $|\psi\rangle_S$ under unitary evolution $U_{S+E}(\phi)$ is given by [3]

$$\begin{aligned}
|\psi\rangle_{S+E} &= N_3 U_P U_{S+E}(\phi) |\psi\rangle_S |0\rangle_E \\
&= N_3 U_{S+E}(\phi) \hat{O} |\psi\rangle_S |0\rangle_E \\
&= N_3 \sum_{l=0}^{\infty} \Pi_l(\phi) \hat{O} |\psi\rangle_S |l\rangle_E \\
&= \sum_{l=0}^{\infty} \Pi_l(\phi) |\Psi\rangle |l\rangle_E,
\end{aligned} \tag{C1}$$

where $|\Psi\rangle = N_3 \hat{O} |\psi\rangle_S$, N_3 is the normalization factor, while \hat{O} represents the equivalent operator that transforms the non-local operation (U_P) into a form preceding the photon losses, with its expression given by $\hat{O} = \frac{\partial^m}{\partial s^m} \exp [s (ae^{i\phi} \sqrt{\eta} \cosh g + b^\dagger \sinh g)] |_{s=0}$ (as shown in Fig. 14). Here, $|0\rangle_E$ represents the initial state in an environment with photon losses, and $|l\rangle_E$ denotes the orthogonal basis corresponding to $|0\rangle_E$. Additionally, $\Pi_l(\phi)$ is the Kraus operator used to describe photon losses, and its form is given by [3]

$$\Pi_l(\phi) = \sqrt{\frac{(1-\eta)^l}{l!}} e^{i\phi(n-\alpha l)} \eta^{\frac{n}{2}} a^l, \tag{C2}$$

where, $e^{i\phi n}$ represents the phase shifter operator. We introduce the parameter α , where $\alpha = 0$ corresponding to photon losses before the phase shifter, and $\alpha = -1$ corresponding to photon losses after the phase shifter. The parameter η represents the transmissivity of the BS that simulating photon losses, with $\eta = 1$ corresponding to a lossless condition.

In the extended system $S + E$, the QFI in the presence of photon losses can be expressed as [3]

$$F_L = C_Q [|\psi\rangle_S, \Pi_l(\phi)]_{\min}. \tag{C3}$$

In this extended system, the upper bound of the QFI is given by [3]

$$\begin{aligned}
C_Q [|\psi\rangle_S, \Pi_l(\phi)] \\
= 4 \left[{}_{S+E} \langle \psi' | \psi' \rangle_{S+E} - |{}_{S+E} \langle \psi' | \psi \rangle_{S+E}|^2 \right].
\end{aligned} \tag{C4}$$

Based on Eqs. (C1) and (C4), $C_Q [|\psi\rangle_S, \Pi_l(\phi)]$ can be expressed as

$$C_Q [|\psi\rangle_S, \Pi_l(\phi)] = 4 \left[\langle h_1 \rangle - |\langle h_2 \rangle|^2 \right], \tag{C5}$$

where $\langle \cdot \rangle = {}_S \langle \psi | \cdot | \psi \rangle_S$, and

$$\begin{aligned}
h_1 &= \sum_{l=0}^{\infty} \frac{dN_3 \hat{O}^\dagger \Pi_l^\dagger(\phi)}{d\phi} \frac{dN_3 \Pi_l(\phi) \hat{O}}{d\phi} \\
&= \frac{dN_3 \hat{O}^\dagger}{d\phi} \frac{dN_3 \hat{O}}{d\phi} + N_3 \hat{O}^\dagger H_1 N_3 \hat{O} \\
&\quad + \frac{dN_3 \hat{O}^\dagger}{d\phi} i H_2^\dagger N_3 \hat{O} + N_3 \hat{O}^\dagger (-i H_2) \frac{dN_3 \hat{O}}{d\phi},
\end{aligned} \tag{C6}$$

$$\begin{aligned}
h_2 &= i \sum_{l=0}^{\infty} \frac{dN_3 \hat{O}^\dagger \Pi_l^\dagger(\phi)}{d\phi} \Pi_l(\phi) N_3 \hat{O} \\
&= i \frac{dN_3 \hat{O}^\dagger}{d\phi} N_3 \hat{O} + N_3 \hat{O}^\dagger H_2 N_3 \hat{O}.
\end{aligned} \tag{C7}$$

where

$$H_1 = \sum_{l=0}^{\infty} \frac{d\Pi_l^\dagger(\phi)}{d\phi} \frac{d\Pi_l(\phi)}{d\phi}, \tag{C8}$$

$$H_2 = i \sum_{l=0}^{\infty} \frac{d\Pi_l^\dagger(\phi)}{d\phi} \Pi_l(\phi). \tag{C9}$$

with H_1, H_2 being expressed by [3]

$$\begin{aligned}
H_1 &= [1 - (1 + \alpha)(1 - \eta)]^2 n^2 \\
&\quad + (1 + \alpha)^2 \eta (1 - \eta) n,
\end{aligned} \tag{C10}$$

$$H_2 = [1 - (1 + \alpha)(1 - \eta)] n. \tag{C11}$$

Based on Eqs. (C2) and (C5)-(C9), $C_Q[|\psi\rangle_S, \Pi_l(\phi)]$ is given by

$$\begin{aligned}
& C_Q[|\psi\rangle_S, \Pi_l(\phi)] \\
&= 4 \left[\langle h_1 \rangle - |\langle h_2 \rangle|^2 \right] \\
&= 4 {}_S \langle \psi | \frac{dN_3 \hat{O}^\dagger}{d\phi} \frac{dN_3 \hat{O}}{d\phi} | \psi \rangle_S \\
&+ 4 {}_S \langle \psi | N_3 \hat{O}^\dagger H_1 N_3 \hat{O} | \psi \rangle_S \\
&+ 4 {}_S \langle \psi | \frac{dN_3 \hat{O}^\dagger}{d\phi} i H_2^\dagger N_3 \hat{O} | \psi \rangle_S \\
&+ 4 {}_S \langle \psi | N_3 \hat{O}^\dagger (-i H_2) \frac{dN_3 \hat{O}}{d\phi} | \psi \rangle_S \\
&- 4 \left| {}_S \langle \psi | i \frac{dN_3 \hat{O}^\dagger}{d\phi} N_3 \hat{O} + N_3^2 \hat{O}^\dagger H_2 \hat{O} | \psi \rangle_S \right|^2 \\
&= 4 \left\langle \tilde{\Psi} | \tilde{\Psi} \right\rangle + 4 \langle \Psi | H_1 | \Psi \rangle \\
&+ 4 \left\langle \tilde{\Psi} | i H_2^\dagger | \Psi \right\rangle - 4 \langle \Psi | i H_2 | \tilde{\Psi} \rangle \\
&- 4 \left| \left(i \langle \tilde{\Psi} | \Psi \right) + \langle \Psi | H_2 | \Psi \right|^2, \tag{C12}
\end{aligned}$$

where $|\tilde{\Psi}\rangle = \partial|\Psi\rangle/\partial\phi$, and $n = a^\dagger a$.

To obtain the $C_Q[|\psi\rangle_S, \Pi_l(\phi)]_{\min}$, we set $\partial C_Q[|\psi\rangle_S, \Pi_l(\phi)]/\partial\alpha = 0$. The expression for the QFI under photon losses is given by

$$\begin{aligned}
F_L &= C_Q[|\psi\rangle_S, \Pi_l(\phi)]_{\min} \\
&= 4 \left[\left\langle \tilde{\Psi} | \tilde{\Psi} \right\rangle - \left| \left\langle \tilde{\Psi} | \Psi \right\rangle \right|^2 \right] \\
&+ \frac{1}{[(1-\eta) \langle \Psi | \Delta n_a^2 | \Psi \rangle + \eta \langle \Psi | n | \Psi \rangle]} \\
&\times [4\eta (\langle \Psi | n | \Psi \rangle) \times (\langle \Psi | \Delta n_a^2 | \Psi \rangle) \\
&+ i \langle \Psi | n | \Psi \rangle \langle \Psi | \tilde{\Psi} \rangle - i \langle \Psi | n | \Psi \rangle \langle \tilde{\Psi} | \Psi \rangle] \\
&+ i \left\langle \tilde{\Psi} | n | \Psi \right\rangle - i \langle \Psi | n | \tilde{\Psi} \rangle \\
&+ (1-\eta) (\langle \tilde{\Psi} | n | \Psi \rangle - \langle \Psi | n | \tilde{\Psi} \rangle) \\
&+ \langle \Psi | n | \Psi \rangle \langle \Psi | \tilde{\Psi} \rangle - \langle \Psi | n | \Psi \rangle \langle \tilde{\Psi} | \Psi \rangle)^2], \tag{C13}
\end{aligned}$$

where

$$\left\langle \tilde{\Psi} | \tilde{\Psi} \right\rangle = N_3^2 \frac{\partial^{2m}}{\partial t^m \partial s^m} (X_2 X_3 - X_4) X_5 |_{s=t=0}, \tag{C14}$$

$$\left\langle \tilde{\Psi} | \Psi \right\rangle = N_3^2 \frac{\partial^{2m}}{\partial t^m \partial s^m} X_2 X_5 |_{s=t=0}, \tag{C15}$$

$$\left\langle \Psi | \tilde{\Psi} \right\rangle = N_3^2 \frac{\partial^{2m}}{\partial t^m \partial s^m} X_3 X_5 |_{s=t=0}, \tag{C16}$$

$$\begin{aligned}
\langle \Psi | n | \Psi \rangle &= N_3^2 \sinh^2 g \\
&\times \frac{\partial^{2m}}{\partial t^m \partial s^m} (X_6 + 1) X_5 |_{s=t=0}, \tag{C17}
\end{aligned}$$

$$\begin{aligned}
\langle \Psi | \Delta n_a^2 | \Psi \rangle &= N_3^2 \sinh^4 g \\
&\times \frac{\partial^{2m}}{\partial t^m \partial s^m} (X_6^2 + 4X_6 + 2) X_5 |_{s=t=0} \\
&+ N_3^2 \sinh^2 g \\
&\times \frac{\partial^{2m}}{\partial t^m \partial s^m} (X_6 + 1) X_5 |_{s=t=0} \\
&- N_3^4 \sinh^4 g \\
&\times \left[\frac{\partial^{2m}}{\partial t^m \partial s^m} (X_6 + 1) X_5 |_{s=t=0} \right]^2, \tag{C18}
\end{aligned}$$

$$\begin{aligned}
\left\langle \tilde{\Psi} | n | \Psi \right\rangle &= N_3^2 \sinh^2 g \\
&\times \frac{\partial^{2m}}{\partial t^m \partial s^m} X_3 (X_6 + 2) X_5 |_{s=t=0}, \tag{C19}
\end{aligned}$$

$$\begin{aligned}
\langle \Psi | n | \tilde{\Psi} \rangle &= N_3^2 \sinh^2 g \\
&\times \frac{\partial^{2m}}{\partial t^m \partial s^m} X_2 (X_6 + 2) X_5 |_{s=t=0}, \tag{C20}
\end{aligned}$$

and

$$N_3 = \left(\frac{\partial^{2m}}{\partial t^m \partial s^m} X_5 |_{s=t=0} \right)^{-\frac{1}{2}}, \tag{C21}$$

as well as

$$X_1 = \frac{1}{2} \sinh 2g \left(-e^{(-i\phi)} \sqrt{\eta} + 1 \right), \tag{C22}$$

$$X_2 = \left(X_1^* - \frac{1}{2} \sinh 2g \right) (is\beta + istX_1), \tag{C23}$$

$$X_3 = \left(\frac{1}{2} \sinh 2g - X_1 \right) (it\beta + itsX_1^*), \tag{C24}$$

$$\begin{aligned}
X_4 &= st \left(\frac{1}{2} \sinh 2g - X_1 \right) \\
&\times \left(X_1^* - \frac{1}{2} \sinh 2g \right), \tag{C25}
\end{aligned}$$

$$X_5 = \exp \left[\beta (sX_1^* + tX_1) + st |X_1|^2 \right], \tag{C26}$$

$$X_6 = (\beta + tX_1) (\beta + sX_1^*). \tag{C27}$$

APPENDIX D : INTERNAL MEAN PHOTON NUMBER

The expression for the average number of internal photons in the equivalent model is given by

$$\begin{aligned}
N_T &= \int_{int} \langle \psi | (a^\dagger a + b^\dagger b) | \psi \rangle_{int} \\
&= N_4^2 \{ \int_{in} \langle \psi | [S_1^\dagger B_1^\dagger U_\phi^\dagger S_2^\dagger a^{\dagger m} S_2 a^\dagger \\
&\quad a S_2^\dagger a^m S_2 U_\phi B_1 S_1] | \psi \rangle_{in} \} \\
&\quad + N_4^2 \{ \int_{in} \langle \psi | [S_1^\dagger B_1^\dagger U_\phi^\dagger S_2^\dagger a^{\dagger m} S_2 b^\dagger \\
&\quad b S_2^\dagger a^m S_2 U_\phi B_1 S_1] | \psi \rangle_{in} \} \\
&= (G_m e^{n_1})^{-1} \times H_m e^{n_2}, \tag{D1}
\end{aligned}$$

where

$$|\psi\rangle_{int} = N_4 S_2^\dagger a^m S_2 U_\phi B_1 S_1 |\psi\rangle_{in} |0\rangle_{a_{v_1}}, \tag{D2}$$

and

$$n_1 = st |v_1|^2 + (sv_1^* + tv_1) \beta, \tag{D3}$$

$$\begin{aligned}
n_2 &= (c \cosh g + sv_1^* + tv_1 + d \cosh g) \beta \\
&\quad + (dv_2^* + sv_1^* + tv_1 + cv_2) \beta \\
&\quad + (tv_1 + cv_2) \times (dv_2^* + sv_1^*) \\
&\quad + sdv_1^* \cosh g + cd \sinh^2 g \\
&\quad + tv_1 (c \cosh g + sv_1^*), \tag{D4}
\end{aligned}$$

as well as

$$v_1 = \frac{1}{2} \sinh 2g (1 - \sqrt{T} e^{-i\phi}), \tag{D5}$$

$$v_2 = -\sqrt{T} \sinh g e^{-i\phi}, \tag{D6}$$

with

$$N_4 = (G_m e^{n_1})^{-\frac{1}{2}}. \tag{D7}$$

-
- [1] V. Giovannetti, S. Lloyd, and L. Maccone, Quantum metrology, *Phys. Rev. Lett.* **96**, 010401 (2006).
- [2] F. Hudelist, J. Kong, C. J. Liu, J. T. Jing, Z. Y. Ou, and W. P. Zhang, Quantum metrology with parametric amplifier-based photon correlation interferometers, *Nat. Commun.* **5**(1), 3049 (2014).
- [3] B. M. Escher, R. L. de Matos Filho, and L. Davidovich, General framework for estimating the ultimate precision limit in noisy quantum-enhanced metrology, *Nat. Phys.* **7**(5), 406–411 (2011).
- [4] J. J. Bollinger, W. M. Itano, D. J. Wineland, and D. J. Heinzen, Optimal frequency measurements with maximally correlated states, *Phys. Rev. A* **54**, R4649 (1996).
- [5] X. Zuo, Z. Yan, Y. Feng, J. Ma, X. Jia, C. Xie, and K. Peng, Quantum interferometer combining squeezing and parametric amplification, *Phys. Rev. Lett.* **124**(17), 173602 (2020).
- [6] R. Birrittella, J. Mimih, and C. C. Gerry, Multiphoton quantum interference at a beam splitter and the approach to Heisenberg-limited interferometry, *Phys. Rev. A* **86**(6), 063828 (2012).
- [7] C. M. Caves, Quantum-mechanical noise in an interferometer, *Phys. Rev. D* **23**, 1693 (1981).
- [8] P. M. Anisimov, G. M. Raterman, A. Chiruvelli, W. N. Plick, S. D. Huver, H. Lee, and J. P. Dowling, Quantum metrology with two-mode squeezed vacuum: parity detection beats the heisenberg limit, *Phys. Rev. Lett.* **104**, 103602 (2010).
- [9] R. Demkowicz-Dobrzański, K. Banaszek, and R. Schnabel, Fundamental quantum interferometry bound for the squeezed-light-enhanced gravitational wave detector GEO 600, *Phys. Rev. A* **88**(4), 041802 (2013).
- [10] J. Aasi, J. Abadie, B. P. Abbott, R. Abbott, T. D. Abbott, M. R. Abernathy, C. Adams, T. Adams, P. Addesso, R. X. Adhikari *et al.*, Enhanced sensitivity of the LIGO gravitational wave detector by using squeezed states of light, *Nat. Photonics* **7**, 613 (2013).
- [11] M. Tse, H. Yu, N. Kijbunchoo, A. Fernandez-Galiana, P. Dupej, L. Barsotti, C. D. Blair, D. D. Brown, S. E. Dwyer, A. Effler *et al.*, Quantum-enhanced advanced LIGO detectors in the era of gravitational-wave astronomy, *Phys. Rev. Lett.* **123**, 231107 (2019).
- [12] C. H. Oh, S. S. Zhou, Y. Wong, and L. Jiang, Quantum limits of superresolution in a noisy environment, *Phys. Rev. Lett.* **126**(12), 120502 (2021).
- [13] M. Tsang, R. Nair, and X. M. Lu, Quantum theory of super-resolution for two incoherent optical point sources, *Phys. Rev. X* **6**(3), 031033 (2016).
- [14] R. Nair and M. Tsang, Interferometric superlocalization of two incoherent optical point sources, *Opt. Express* **24**(4), 3684–3701 (2016).
- [15] M. A. Taylor, J. Janousek, V. Daria, J. Knittel, B. Hage, H.-A. Bachor, and W. P. Bowen, Biological measurement beyond the quantum limit, *Nat. Photonics* **7**, 229 (2013).
- [16] M. A. Taylor and W. P. Bowen, Quantum metrology and its application in biology, *Phys. Rep.* **615**, 1 (2016).
- [17] S. L. Braunstein and P. V. Loock, Quantum information with continuous variables, *Rev. Mod. Phys.* **77**(2), 513–577 (2005).
- [18] V. Giovannetti, S. Lloyd, and L. Maccone, Quantum-enhanced measurements: Beating the standard quantum limit, *Science* **306**(5700), 1330–1336 (2004).
- [19] V. Giovannetti, S. Lloyd, and L. Maccone, Advances in quantum metrology, *Nat. Photonics* **5**(4), 222–229 (2011).
- [20] Z. Y. Ou and X. Li, Quantum SU(1,1) interferometers: Basic principles and applications, *APL Photonics* **5**(8), 080902 (2020).
- [21] Y. K. Xu, S. K. Chang, C. J. Liu, L. Y. Hu, and S. Q. Liu, Phase estimation of an SU(1,1) interferometer with a coherent superposition squeezed vacuum in a realistic case, *Opt. Express* **30**(21), 38178(2022).
- [22] D. Li, B. T. Gard, Y. Gao, C. H. Yuan, W. P. Zhang, H. Lee, and J. P. Dowling, Phase sensitivity at the Heisenberg limit in an SU(1,1) interferometer via parity detection, *Phys. Rev. A* **94**(6), 063840 (2016).
- [23] C. W. Helstrom, Quantum detection and estimation theory, (Academic, 1976), Vol. 123.

- [24] M. J. Holland and K. Burnett, Interferometric detection of optical phase shifts at the Heisenberg limit, *Phys. Rev. Lett.* **71**, 1355 (1993).
- [25] Z. Y. Ou, Complementarity and fundamental limit in precision phase measurement, *Phys. Rev. Lett.* **77**, 2352 (1996).
- [26] J. Joo, W. J. Munro, and T. P. Spiller, Quantum metrology with entangled coherent states, *Phys. Rev. Lett.* **107**, 083601 (2011).
- [27] Y. Israel, S. Rosen, and Y. Silberberg, Supersensitive polarization microscopy using NOON states of light, *Phys. Rev. Lett.* **112**, 103604 (2014).
- [28] R. A. Campos, C. C. Gerry, and A. Benmoussa, Optical interferometry at the Heisenberg limit with twin Fock states and parity measurements, *Phys. Rev. A* **68**, 023810 (2003).
- [29] T. Ono and H. F. Hofmann, Effects of photon losses on phase estimation near the Heisenberg limit using coherent light and squeezed vacuum, *Phys. Rev. A* **81**, 033819 (2010).
- [30] Z. K. Zhao, H. Zhang, Y. B. Huang, and L. Y. Hu, Phase estimation of a Mach-Zehnder interferometer via the Laguerre excitation squeezed state, *Opt. Express* **31**, 17645 (2023).
- [31] H. Zhang, W. Ye, C. P. Wei, C. J. Liu, Z. Y. Liao, and L. Y. Hu, Improving phase estimation using number-conserving operations, *Phys. Rev. A* **103**(5), 052602 (2021).
- [32] Y. K. Xu, T. Zhao, Q. Q. Kang, C. J. Liu, L. Y. Hu, and S. Q. Liu, Phase sensitivity of an SU(1,1) interferometer in photo-loss via photon operations, *Opt. Express* **31**(5), 8414(2023).
- [33] Q. K. Gong, X. L. Hu, D. Li, C. H. Yuan, Z. Y. Ou, and W. P. Zhang, Intramode-correlation-enhanced phase sensitivities in an SU(1,1) interferometer, *Phys. Rev. A* **96**(3), 033809 (2017).
- [34] S. Ataman, Optimal Mach-Zehnder phase sensitivity with Gaussian states, *Phys. Rev. A* **100**, 063821 (2019).
- [35] B. Yurke, S. L. McCall, and J. R. Klauder, SU(2) and SU(1,1) interferometers, *Phys. Rev. A* **33**(6), 4033–4054 (1986).
- [36] J. D. Zhang, C. L. You, C. Li, and S. Wang, Phase sensitivity approaching the quantum Cramér-Rao bound in a modified SU(1,1) interferometer, *Phys. Rev. A* **103**, 032617 (2021).
- [37] K. Zhang, Y. H. Lv, Y. Guo, J. T. Jing, and W. M. Liu, Enhancing the precision of a phase measurement through phase-sensitive non-Gaussianity, *Phys. Rev. A* **105**, 042607 (2022).
- [38] J. Kong, Z. Y. Ou, and W. P. Zhang, Phase-measurement sensitivity beyond the standard quantum limit in an interferometer consisting of a parametric amplifier and a beam splitter, *Phys. Rev. A* **87**, 023825 (2013).
- [39] O. Seth, X. F. Li, H. N. Xiong, J. Y. Luo, and Y. X. Huang, Improving the phase sensitivity of an SU(1,1) interferometer via a nonlinear phase encoding, *J. Phys. B: At., Mol. Opt. Phys.* **53**(20), 205503 (2020).
- [40] S. K. Chang, W. Ye, H. Zhang, L. Y. Hu, J. H. Huang, and S. Q. Liu, Improvement of phase sensitivity in an SU(1,1) interferometer via a phase shift induced by a Kerr medium, *Phys. Rev. A* **105**(3), 033704 (2022).
- [41] S. Ataman, Quantum Fisher information maximization in an unbalanced interferometer, *Phys. Rev. A* **105**, 012604 (2022).
- [42] S. Ataman, K. K. Mishra, Quantum Fisher information maximization in an unbalanced lossy interferometer, *Phys. Rev. A* **109**, 062605 (2024).
- [43] M. Jarzyna, R. Demkowicz-Dobrzanski, Quantum interferometry with and without an external phase reference, *Phys. Rev. A* **85**, 011801 (2012).
- [44] S. S. Liu, Y. B. Lou, J. Xin, and J. T. Jing, Quantum enhancement of phase sensitivity for the bright-seeded SU(1,1) interferometer with direct intensity detection, *Phys. Rev. Appl.* **10**(6), 064046 (2018).
- [45] M. Manceau, G. Leuchs, F. Khalili, and M. Chekhova, Detection loss tolerant supersensitive phase measurement with an SU(1,1) interferometer, *Phys. Rev. Lett.* **119**(22), 223604 (2017).
- [46] W. Du, J. Jia, J. F. Chen, Z. Y. Ou, and W. P. Zhang, Absolute sensitivity of phase measurement in an SU(1,1) type interferometer, *Opt. Lett.* **43**(5), 1051 (2018).
- [47] S. S. Szigeti, R. J. Lewis-Swan, and S. A. Haine, Pumped-up SU(1,1) interferometry, *Phys. Rev. Lett.* **118**, 150401 (2017).
- [48] D. Li, C. H. Yuan, Z. Y. Ou, and W. P. Zhang, The phase sensitivity of an SU(1,1) interferometer with coherent and squeezed-vacuum light, *New J. Phys.* **16**(7), 073020 (2014).
- [49] N. Namekata, Y. Takahashi, G. Fujii, D. Fukuda, S. Kurimura, and S. Inoue, Non-Gaussian operation based on photon subtraction using a photon-number-resolving detector at a telecommunications wavelength, *Nat. Photon.* **4**, 655 (2010).
- [50] G. S. Agarwal and K. Tara, Nonclassical properties of states generated by the excitations on a coherent state, *Phys. Rev. A* **43**, 492 (1991).
- [51] L. Y. Hu and Z. M. Zhang, Statistical properties of coherent photon-added two-mode squeezed vacuum and its inseparability, *J. Opt. Soc. Am. B* **30**, 518 (2013).
- [52] A. Zavatta, V. Parigi, and M. Bellini, Experimental non-classicality of single-photon-added thermal light states, *Phys. Rev. A* **75**, 052106 (2007).
- [53] Y. Ouyang, S. Wang, and L. J. Zhang, Quantum optical interferometry via the photon-added two-mode squeezed vacuum states, *J. Opt. Soc. Am. B* **33**, 1373 (2016).
- [54] J. Xin, Phase sensitivity enhancement for the SU(1,1) interferometer using photon level operations, *Opt. Express* **29**(26), 43970(2021).
- [55] M. Dakna, L. Knöll, and D.-G. Welsch, Photon-added state preparation via conditional measurement on a beam splitter, *Opt. Commun.* **145**(1-6), 309–321 (1998).
- [56] L. L. Guo, Y. F. Yu, and Z. M. Zhang, Improving the phase sensitivity of an SU(1,1) interferometer with photon-added squeezed vacuum light, *Opt. Express* **26**(22), 29099 (2018).
- [57] X. Y. Hu, C. P. Wei, Y. F. Yu, and Z. M. Zhang, Enhanced phase sensitivity of an SU(1,1) interferometer with displaced squeezed vacuum light, *Front. Phys.* **11**, 114203 (2016).